Unloading Response Characteristics of Cross Fault Caverns: Effect of Fault Angles

Yong-Hui Shang (syhsrsci@sina.com)
Central South University
Lin-Rong Xu
Huanghuai University
Yong-Wei Li
Central South University

Research Article

Keywords: Caverns, Unloading response, Particle flow code, Acoustic emission, Energy, Failure modes

Posted Date: May 28th, 2021

DOI: https://doi.org/10.21203/rs.3.rs-523809/v1

Version of Record: A version of this preprint was published at Geotechnical and Geological Engineering on July 20th, 2021. See the published version at https://doi.org/10.1007/s10706-021-01942-5.

Abstract

The research of unloading response characteristics of caverns with weak structure has important engineering value for the development and construction of underground space. In this paper, firstly, the cross fault cavity model is established based on particle flow code (PFC) software, considering different fault dip angles. The parallel bond model (PBM) is used in the cavern model and the smooth joint model (SJM) is used in the fault model. Then, the mechanical, acoustic emission (AE), energy response characteristics and failure modes of the cavern model with different fault angles are explored. The research result show that the fault angle has a great influence on the stress distribution and failure modes of surrounding rock.The existence of faults does not change the overall law of AE evolution curve, that is, the number of AE hits increases first and then decreases. However, the existence of faults changes the maximum number of AE hits and the duration of AE. When the cavern is unloaded, the strain energy of the model first decreases and then increases.

Introduction

With the development of economy and the increase of population, the development scale and depth of underground tunnel engineering are increasing (Wang et al, 2020; Zhao et al, 2021). At present, the deepest tunnel project in the world has reached 1500m. Meanwhile, the construction of underground tunnel will inevitably encounter weak geological structures such as faults, which makes the unloading response characteristics of surrounding rock more complex and more likely to induce tunnel dynamic disasters, such as rock burst (Ortlepp and Stacey, 1994; He et al, 2010; Manouchehrian and Cai, 2015). Therefore, it is of great engineering significance to study the unloading response characteristics of cross fault caverns for the safety control of underground space.

Many scholars have done a lot of research work and made great achievements in the mechanical properties of unloading rock mass. The unloading deformation behavior and failure characteristics of rock were studied by Huang et al (2001) by experiments. Their result show that rock bursts occur in the unloading process of tunnel excavation and their characteristics are closely related to the deformation and failure characteristics of the rock mass. Based on the field test and numerical simulation, Sharma et al (2001) analyzed the influence of Large Space Excavation on the deformation of adjacent tunnels. It was found that the stiffness of the tunnel lining has significant influence on the displacement and distortion of tunnels caused by an adjacent excavation. A stiffer lining undergoes less displacement and distortion but is likely to experience significantly greater bending moments. Kojima and Yashiro (2005) established a method to evaluate the deformation characteristics of tunnel under the action of embankment and surface excavation through surface loading and unloading model test. The results show that the nonlinear deformation behavior of M-type tunnel is obvious in loading test, and that of S-type tunnel is obvious in unloading test. The larger the B / H is, the more obvious the deformation behavior is. Based on the theory and numerical simulation, Li et al (2016) studied the dynamic response of unloading times, stress level and tunnel spacing configuration to the surrounding rock of the existing tunnel. The results show that under the condition of high initial stress and high unloading rate, the

surrounding rock of existing tunnel will produce dynamic effect. The particle peak velocity (PPV) induced by unloading can reach the PPV value induced by blasting and damage the existing tunnel. Chen et al. (2020) studied the failure characteristics of deep circular tunnel in rock mass with multiple weak surfaces by using two-dimensional combined finite element method / discrete element method (FEM / DEM). Then, parametric analysis is carried out to study the effects of dip angle and length on crack propagation behavior, failure mode, energy evolution and displacement distribution. The results show that the inclination angle has a great influence on the stability of the tunnel, and the failure strength and range first increase and then decrease with the increase of the inclination angle. With the increase of the length of weak surface, the possibility of dynamic disaster increases. These studies are of great significance for the prevention and control of tunnel unloading disasters. However, these studies did not consider the influence of fault on the response characteristics of tunnel during excavation.

In addition, the damage of surrounding rock is often accompanied by acoustic emission (AE), which can be used to predict and control rockburst and other disasters (Přikryl et al, 2003; Shkuratnik et al, 2005; Wang et al, 2018). The energy evolution characteristics of the surrounding rock can better reflect the essence of the instability failure of the cavern (Persson, 1997; Chen et al, 2021). Therefore, this paper not only analyzes the unloading failure mechanics and instability characteristics of cross fault cavern, but also analyzes the acoustic emission and energy evolution characteristics of surrounding rock. The specific contents are as follows: firstly, based on PFC, the cross fault cavity models with different fault dip angles are established, and the parameters are checked; Secondly, the mechanics, acoustic emission, energy and instability behavior or characteristics of the cross fault cavern are analyzed. The research results are helpful to further understand the unloading response characteristics of cross fault caverns and disaster prevention and control.

Numerical Model Of Cross Fault Cavern

2.1 Numerical method

Based on discrete medium mechanics, the particle flow code (PFC) adopts the combination of meso particles to form a macro material. The macro and meso mechanical behavior of material is expressed through the movement and interaction of particles, which overcomes the macro continuity assumption of traditional continuum mechanics model, and is suitable for simulating materials composed of mineral particles (Itasca Consulting Group Inc. 2014). According to the model function of the particle flow program and the research results of Chen et al (2020), the bond in the parallel bond model (Fig. 1a) acts on a finite size circular section between two particles, which can transfer force and torque, and has been widely used to simulate the mechanical properties of rock like materials, In this paper, the parallel bond model is used to establish the surrounding rock model.

For weak structures such as faults, the smooth joint model (as shown in Fig. 1b) can be used for simulation (Itasca Consulting Group Inc. 2014). The smooth joint model simulates the behavior of the plane interface with dilation, which is independent of the local particle contact direction on the interface.

The behavior of friction or bond joints can be modeled by assigning a smooth joint model to all contacts between particles on the opposite side of the joint. The smooth joint model provides the macroscopic behavior of linear elasticity and the bonding or friction interface with expansion. The behavior of the bonded interface is linear elastic until the strength limit is exceeded, and the interface is unbonded. The behavior of unbonded interface is linear elasticity and friction with dilation, with slip accommodated by imposing a Coulomb limit on the shear force. The interface is not resistant to relative rotation (MC ≡ 0).

2.2 Model parameters

In PFC, the macro-mechanical property of the rock model is determined by the micro-mechanical property of the particles and bonds. However, these parameters cannot be directly derived directly from in-situ tests and indoor experiments. Usually, the micro-parameters of PFC rock models are calibrated by simulating the uniaxial compression experiments. Generally, the method of trial and error is often used to check the parameters of indoor test scale samples, and the specific process can refer to the literature provided by Castro-Filgueira et al (2017). However, for tunnels or other huge models, the scale level is meter (m). If the parameters of the indoor small-scale model are used to establish the arge-scale model, the number of particles of largescale model needs tens of millions, and the general computer can not load. For this reason, we consider the scale effect of the model in the parameter verification. Through lab tests, Li et al (2020) found that when the scale of the model is larger than 80mm, the uniaxial compressive strength of the shale decreases by more than 40%, that is, from 80MPa to 48mpa. The elastic modulus is 4–8 GPa. Combined with this information, uniaxial compression experiments were carried out on rock samples with model size of 20m * 40m by trial and error method, and the parameters were checked repeatedly to obtain the meso parameters of PFC that can reflect the mechanical properties of shale, as shown in Table 1. Under this parameters, the compressive strength of rock mass is about 46.9 MPa and the elastic modulus is about 4.2 GPa, as shown in Fig. 2. The failure mode, as shown in Fig. 3a, is mainly in the split at the end and middle of the sample, which is consistent with the failure model of the large-scale model of indoor experiment, Fig. 3b.

Table 1
Physico-mechanical parameters of numerical test model

Parameter	Value	Parameter	Value
Minimum particle diameter (mm)	300	Porosity	0.1
Maximum particle diameter (mm)	400	Density (kg/m^3)	2600
Contact modulus of the particle (GPa)	4.2	Parallel bond tensile strength (MPa)	18
Parallel bond Deformation modulus (GPa)	4.2	Parallel bond Cohesive force (MPa)	27
Contact bond gap (mm)	0.05	Stiffness ratio	1.25

Because it is difficult to measure the mechanical properties of the fault, the value of the meso parameters of the fault in this paper is 5% of the surrounding rock parameters according to research of Chen et al (2021), as shown in Table 2.

Table 2
Physico-mechanical parameters of fault

Parameter	Value	Parameter	Value
Joint tensile strength (MPa)	0.9	Joint normal stiffness (GPa/m)	1
Joint cohesive force (MPa)	1.35	Joint tangential stiffness (GPa/m)	1
Joint friction coefficient	0.3	Joint width (mm)	1

2.3 Numerical models

According to the engineering practice, the scale of the model is 60m * 60m, as shown in Fig. 4; The diameter of the cavern is 12m; There is a fault with a length of 40m passing through the center of the cavern. The angle between the fault and the X-axis is *a*, which is the fault angle. Because this paper mainly studies the influence of fault angle on the unloading response characteristics of surrounding rock, the fault angle is set to 0 °, 30°, 60 °, 90 °, 120 ° and 150 °, as shown in Fig. 5. The model considers the deep buried geological conditions, the buried depth is 1500m, the vertical confining pressure of the cavern is 39Mpa, and the side pressure coefficient is 0.5. The process of model establishment: firstly, the rectangular surrounding rock model is generated, and then the confining pressure is applied; secondly, the fault model is added and the cavern is removed for unloading. Before the run of the model, four measuring circle with a diameter of 2m was established at the top, bottom, left and right sides of the cavern model to record the stress evolution process of surrounding rock mass. At the same time, the acoustic emission characteristics and energy characteristics of the whole model are recorded by writing FISH Language.

Results

3.1 Stress response characteristics of surrounding rock

Figure 6 show the stress response characteristics of surrounding rock of cavern without fault. It can be seen from the figure that after unloading, the stress of points M1 and M2 in the Y direction suddenly decreases, which is due to the loss of supporting rock mass due to the excavation of the cavern. For point M3 and point M4, they bear the initial stress of point M1 and point M2, showing a sudden increase of stress concentration. At the same time, the stress state of point M3 and point M4 is not the same due to the inhomogeneity of rock particle medium. On the contrary, in the X direction, the stress of point M3 and point M4 shows a downward trend, while the stress concentration occurs at point M1 and point M2.

Figure 7–8 and Table 3 show the stress response characteristics and maximum stress of the cross fault cavern under unloading. The angle of fault changes the unloading stress state of surrounding rock and has a great influence on the stability of the cavern. For the stress in Y direction, the change of point M1 and point M2 is small. The stress reduction of the fault with angle 90° is due to the fact that the fault crosses the measuring circle. This means the fault with angle 90° will lead to the large unloading stress at the top of the cavern in Y direction. At point M3, except fault with angle 60° and 90° result in the increase of stress, the stress of point M3 decreases due to the faults of other angles. The maximum

stress of point M3 without fault, with fault angle = 0°, 30°, 60°, 90°, 120°, and 150° are 71MPa, 66.7MPa, 64.2MPa, 72.1MPa, 71.3MPa, 67.1MPa and 67.4MPa. At point M4, except for the fault angle of 90°, the stress at point m3 decreases. The maximum stress of point M4 without fault, with fault angle = 0°, 30°, 60°, 90°, 120°, and 150° are 71MPa, 69.1MPa, 62.6MPa, 67.6MPa, 71.2MPa, 70.8 and 65.1MPa. Generally, the existence of fault will lead to the decrease of unloading stress (Y direction) at the arch waist of the cavern, especially when the fault angle is about 60°.

For the stress in X direction, the point M1-M4 changes greatly due to the existence of faults. At point M1, the fault angle is 0°, 90° will lead to stress increase, while other angles will lead to stress decrease. When the fault angle is 120°, the stress reduction is the largest. When the fault angle is 0°, the stress increases most. The maximum stress of point M1 without fault, with fault angle = 0°, 30°, 60°, 90°, 120°, and 150° are 31.1MPa, 34.6MPa, 29.5MPa, 25MPa, 33.9MPa, 24MPa and 19.6MPa. At point M2, a fault angle of 30° will increase the stress, while other angles will decrease the stress. When the fault angle is 60°, the stress reduction is the largest. The maximum stress of point M2 without fault, with fault angle = 0°, 30°, 60°, 90°, 120°, and 150° are 32.2MPa, 34.7MPa, 31.2MPa, 25.4MPa, 31.6MPa, 26.5MPa and 30.1MPa. At point M3, fault angles of 0°, 60° and 90° lead to stress increase, while other angles lead to stress decrease. When the fault angle is 0°, the stress increases most. When the fault angle is 30° or 150°, the stress reduction is the largest. The maximum stress of point M3 without fault, with fault angle = 0°, 30°, 60°, 90°, 120°, and 150° are 9.1MPa, 13.5MPa, 8.5MPa, 9.9MPa, 9.4MPa, 8.5MPa and 9.8MPa. At point M4, the fault angle is 0°, 90° will lead to stress increase, while other angles will lead to stress decrease. When the fault angle is 0°, the stress increases most. When the fault angle is 150°, the stress reduction is the largest. The maximum stress of point M4 without fault, with fault angle = 0°, 30°, 60°, 90°, 120°, and 150° are 16.6MPa, 18.4MPa, 12.7MPa, 16.7MPa, 17.7MPa, 15.2MPa and 11.7MPa. It can be seen that the fault angle has great influence on the X direction of surrounding rock, especially when the fault angle is 0° and 90°. At the same time, the fault angles of 30° and 90° can reduce the stress concentration of surrounding rock in X direction.

In general, the fault angle has a great influence on the stress distribution of surrounding rock. Faults with angles of 0° and 90° will increase the stress concentration of surrounding rock (except for some points), while faults with other angles will reduce the stress concentration of surrounding rock.

Table 3
Maximum stress of monitoring points

Maximum Stress	M1-X	M2-X	M3-X	M4-X	M1-Y	M2-Y	M3-Y	M4-Y
No fault	31.1	32.2	9.1	16.6	8.2	9.1	71	71
Fault angle = 0°	34.6	34.7	13.5	18.4	9.3	10.1	66.7	69.1
Fault angle = 30°	29.5	31.2	8.5	12.7	8.1	9.2	64.2	62.6
Fault angle = 60°	25	25.4	9.9	16.7	7.6	8.1	72.1	67.6
Fault angle = 90°	33.9	31.6	9.4	17.7	13.3	16.2	71.3	71.2
Fault angle = 120°	24	26.5	8.5	15.2	7.5	8.4	67.1	70.8
Fault angle = 150°	29.6	30.1	9.8	11.7	8	9.1	67.4	65.1

Note: Mi-X represent the stress of monitoring points in X direction and Mi-Y represent the stress of monitoring points in Y direction, i = 1, 2, 3, 4.

3.2 AE characteristics

The acoustic emission (AE) characteristics of rock mass is directly related to the generation of micro cracks in the rock mass. In the PFC model, a contact (parallel bond) fracture will produce a release of strain energy, that is, an acoustic emission occurs. Therefore, the acoustic emission event of rock sample can be simulated by counting the number of particle contact fractures through FISH language (Chen et al, 2021). Figure 9 shows the evolution characteristics of acoustic emission during unloading of faultless caverns. It can be seen from the figure that in the process of sudden unloading, a large number of acoustic emission hits events occurred in the surrounding rock of the cavern. The maximum value of acoustic emission hit event is 6, and there are two peaks, which is due to two times of rapid crack propagation in surrounding rock. At the same time, it can also be seen that the number of acoustic emission hits increases first and then decreases, which indicates that the stress concentration of the cavern needs a process. After the stress concentration leads to the damage and failure of the rock mass, it returns to the stable state of the surrounding rock, which is consistent with the stress evolution curve in Fig. 6.

Figure 10 shows the AE evolution curves of surrounding rock under different fault angles. Generally, the existence of faults does not change the overall law of AE evolution curve, that is, the number of AE hits increases first and then decreases. However, the existence of faults changes the maximum number of AE hits and the duration of AE. Compared with the AE characteristics of no fault cavern, the maximum hit value of AE increases when the fault dip angle is 30° and 120°. The difference is that when the fault angle is 30°, the duration of AE hit event is longer, while the duration of AE hit event of 120° fault cavern model is slightly shorter. The maximum hit value of AE of the tunnel model with fault angle of 90° is the same as that of the tunnel model without fault, both are 6, but the duration of AE hit increases. The results show that the maximum value of AE hits is smaller and the duration of AE hits is shorter when the fault angle is 0°, 60° and 150°. These phenomena indicate that the existence of faults affects the crack

development of caverns. In general, the maximum hit value of AE increases when the fault dip angle is 30° and 120°, while other angles decrease. The number of AE hits caused by the fault angle of 30° is the most, about 134 times, which is 31 times more than that of the no fault cavern model. The number of AE hits is 104 times for the model with 90° fault, which is one more than that of the model without fault. The total number of AE hits in other fault models decreased. The number of AE hits of the cavity model with fault angles of 0°, 60°, 120° and 150° are 49 times, 85 times, 78 times and 45 times.

3.3 Strain energy characteristics

The law of thermodynamics shows that energy conversion is the intrinsic essence of the change process of physical characteristics of materials. When the sample is loaded, part of the work done by the loading plate is used for the internal damage, plastic deformation and crack propagation of rock, which is called dissipation energy. The other part is stored in the rock in the form of strain energy. From the energy point of view, the damage and fracture of the specimen is the result of energy accumulation and transformation process such as internal strain energy and dissipation energy. Many studies (Xie et al, 2004; Ma et al, 2020) show that the analysis of strain energy is helpful to understand the instability mechanism of rock mass and control the stability of rock mass.

In the PFC model, the strain energy consists of two parts: the strain energy E_K and the parallel bonding strain energy $\overline{E}_K$, i.e,

$$U_E = E_K + \overline{E}_K \quad (1)$$

$$E_K = \frac{1}{2}\left(\frac{\left(F_n^I\right)^2}{k_n} + \frac{\left\|F_s^I\right\|^2}{k_s} \right) \quad (2)$$

$$\overline{E}_K = \frac{1}{2}\left(\frac{\overline{F}_n^2}{\overline{k}_n \overline{A}} + \frac{\left\|\overline{F}_s\right\|^2}{\overline{k}_s \overline{A}} + \frac{\overline{M}_t^2}{\overline{k}_s \overline{J}} + \frac{\left\|\overline{M}_b\right\|^2}{\overline{k}_n \overline{I}} \right) \quad (3)$$

where, F_n^I and F_s^I are the normal and tangential contact forces of particles; k_n and K_s are the normal and tangential contact stiffness of particles; $\overline{F}_n$ and $\overline{F}_s$ andare the normal and tangential parallel bond forces; $\overline{k}_n$ and $\overline{K}_s$ are the normal and tangential parallel bond stiffness; $\overline{M}_t$ and $\overline{M}_b$ are the torque and bending moment of parallel bonding; $\overline{A}$ is the area of parallel bonding; $\overline{J}$ and $\overline{I}$ are the polar moment of inertia and moment of inertia of parallel bonded section.

Through the fish language built in PFC, the strain energy can be monitored in real time.

Figure 11 shows the strain energy characteristics of caverns with and without faults. Due to the confining pressure, a large amount of strain energy, about 32e7J, is accumulated in the early stage before unloading. When the cavern is unloaded, the strain energy of the model first decreases and then increases, because the energy in the rock mass is dissipated due to the sudden release of excavation space. However, with the stress re-distribution of surrounding rock, the strain energy of the whole model increases. Compared with the non-fault cavern model, the strain energy attenuation of the cross fault cavern model (in the early unloading stage) is larger, and the strain energy increment in the later unloading stage is also larger. This is because of the existence of faults, the deformation space and amount of the whole model are increased. In general, the strain energy increment of the cavern model with 0° and 30° fault angles are the largest, followed by 150°, 60°, 120° and 90 °.

3.4 Failure modes

Figure 12 show the failure modes of cavern with different fault angles. It can be seen from the figure that in the case of cavern without fault, the damage of the cavern is mainly in the arch waist of the cavern. This is because the lateral pressure coefficient of the model is 0.5. The failure degree of the left and right sides of the tunnel is different because the model is a discrete element body. Compared with no fault cavern, the failure mode of cross fault cavern has changed greatly. When the fault angle is 0°, the damage of the cavern is transferred to the left arch waist of the cavern, and the overall damage of the cavern is smaller than that of the non-fault cavern. When the fault angle is 30°, the damage degree of the cavern is more severe, and the damage location is still mainly in the right arch waist of the cavern. When the fault dip angle is 60° and 90°, the failure mode of the cavern is basically consistent with that of the non-fault cavern model. When the fault angle is 120° and 150°, the damage degree of the cavern is less than that of the non-fault cavern. In general, the failure degree of the cavern model decreases when the fault angle is 0°, 120 ° and 150°, while the failure degree increases when the fault angle is 30°.

Conclusions

Based on the PFC model, the mechanical, acoustic emission and energy response characteristics of the cross fault cavern are analyzed, and the influence of joint angle is considered. At the same time, the failure modes of each model are analyzed. The main conclusions of this paper are as follow:

The fault angle has a great influence on the stress distribution of surrounding rock. Faults with angles of 0° and 90° will increase the stress concentration of surrounding rock, while faults with other angles will reduce the stress concentration of surrounding rock.

The existence of faults does not change the overall law of AE evolution curve, that is, the number of AE hits increases first and then decreases. However, the existence of faults changes the maximum number of AE hits and the duration of AE. Compared with the AE characteristics of no fault cavern, the maximum hit value of AE increases when the fault dip angle is 30° and 120°. When the fault angle is 30°, the duration of AE hit event is longer, while the duration of AE hit event of 120° fault cavern model is slightly shorter. The maximum hit value of AE of the tunnel model with fault angle of 90° is the same as that of

the tunnel model without fault, both are 6, but the duration of AE hit increases. The maximum value of AE hits is smaller and the duration of AE hits is shorter when the fault angle is 0°, 60° and 150°.

When the cavern is unloaded, the strain energy of the model first decreases and then increases. Compared with the non-fault cavern model, the strain energy attenuation of the cross fault cavern model (in the early unloading stage) is larger, and the strain energy increment in the later unloading stage is also larger. The strain energy increment of the cavern model with 0° and 30° fault angles are the largest, followed by 150°, 60°, 120° and 90 °.

Compared with no fault cavern, the failure mode of cross fault cavern has changed greatly. The failure degree of the cavern model decreases when the fault angle is 0°, 120 ° and 150°, while the failure degree increases when the fault angle is 30°.

Declarations

Data Availability

The data used to support the findings of this study are included within the article.

Conflict of interest

The authors declare that they have no conflicts of interest.

Acknowledgements

This work is financially supported by the National Natural Science Foundation of China (grant number 51778634), Postdoctoral Science Foundation Project of China(2020M682589), Key Projects Supported by Henan Provincial Education Department in Henan Province of China (grant number 20B580003), and Scientific and Technological Research Projects in Henan Province of China (grant number 202102310264). The contributions of anonymous reviewers and editors are also acknowledged.

ORCID

Yong-Hui Shang https://orcid.org/0000-0003-2231-3094

Yong-Wei Li https://orcid.org/0000-0002-2030-0815

References

1. Castro-Filgueira U, Alejano L R, Arzúa J, et al (2017) Sensitivity analysis of the micro-parameters used in a PFC analysis towards the mechanical properties of rocks. Procedia Engineering, 191: 488-495.
2. Chen Z, Xu L, Shang Y (2021) Influence of Joint Angle on the Acoustic Emission Evolution Characteristics and Energy Dissipation Rule of Rock Mass. Geotechnical and Geological Engineering,

39(2): 1621-1635.

3. Chen S, Feng F, Wang Y, et al (2020) Tunnel failure in hard rock with multiple weak planes due to excavation unloading of in-situ stress. Journal of Central South University, 27(10): 2864-2882.
4. Huang R Q, Wang X N, Chan L S (2001) Triaxial unloading test of rocks and its implication for rock burst. Bulletin of Engineering Geology and the Environment, 60(1): 37-41.
5. He M C, Miao J L, Feng J L (2010) Rock burst process of limestone and its acoustic emission characteristics under true-triaxial unloading conditions. International Journal of Rock Mechanics and Mining Sciences, 47(2): 286-298.
6. Itasca Consulting Group (2014) PFC Users' Manual (version 5.0). Minnestota: Inc.
7. Kojima Y, Yashiro K (2005) Deformation behavior of tunnel lining due to ground surface loading and unloading above the tunnel. Quarterly Report of RTRI, 46(2): 143-146.
8. Li X, Cao W, Tao M, et al (2016) Influence of unloading disturbance on adjacent tunnels. International Journal of Rock Mechanics and Mining Sciences, 84: 10-24.
9. Li Shuai, Chen Junbin, Wang Hanqing, et al (2020) Experimental study on the scale effect of strength and deformation of Chang 7 shale in Ordos Basin. Journal of China Coal Society, 45(12) : 4121-4131.
10. Manouchehrian A, Cai M (2015) Simulation of unstable rock failure under unloading conditions. Canadian Geotechnical Journal, 53(1): 22-34.
11. Ma Q, Tan Y, Liu X, Gu Q, Li X (2020) Effect of coal thicknesses on energy evolution characteristics of roof rock-coal-floor rock sandwich composite structure and its damage constitutive model. Composites Part B, 198:108086.
12. Ortlepp W D, Stacey T R (1994) Rockburst mechanisms in tunnels and shafts. Tunnelling and Underground Space Technology, 9(1): 59-65.
13. Persson P A. (1997) The relationship between strain energy, rock damage, fragmentation, and throw in rock blasting. Fragblast, 1(1): 99-110.
14. Přikryl R, Lokajíček T, Li C, et al (2003) Acoustic emission characteristics and failure of uniaxially stressed granitic rocks: the effect of rock fabric. Rock Mechanics and Rock Engineering, 36(4): 255-270.
15. Shkuratnik V L, Filimonov Y L, Kuchurin S V (2005) Regularities of acoustic emission in coal samples under triaxial compression. Journal of Mining Science, 41(1): 44-52.
16. Sharma J S, Hefny A M, Zhao J, et al (2001) Effect of large excavation on deformation of adjacent MRT tunnels. Tunnelling and Underground Space Technology, 16(2): 93-98.
17. Wang X, Wen Z, Jiang Y, et al (2018) Experimental study on mechanical and acoustic emission characteristics of rock-like material under non-uniformly distributed loads. Rock Mechanics and Rock Engineering, 51(3): 729-745.
18. Wang X, Wu N, Li H, et al (2020) Influence of joint angle on the instability failure characteristics and AE evolution law of underground caverns. European Journal of Environmental and Civil Engineering,

1-18.

19. Zhao Z, Sun W, Chen S, et al (2021) Determination of critical criterion of tensile-shear failure in Brazilian disc based on theoretical analysis and meso-macro numerical simulation, Computers and Geotechnics, Volume 134, 104096,

Figures

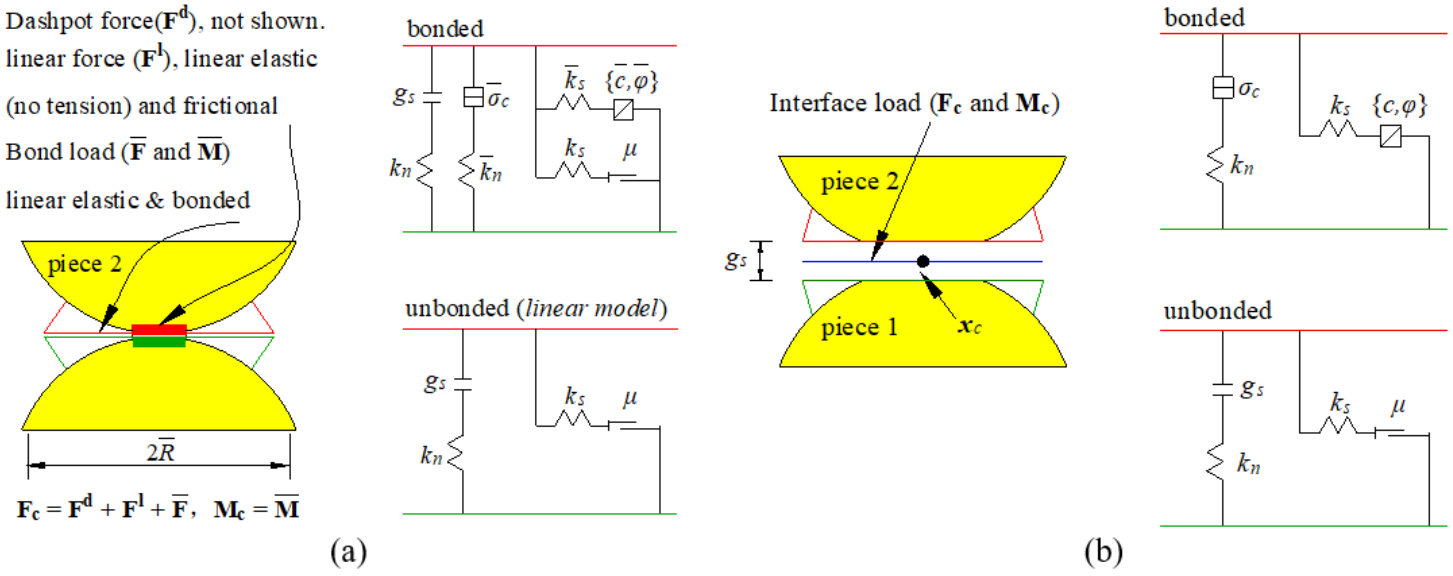

Figure 1

Parallel bond model (a) and smooth joint model (b) (Itasca Consulting Group Inc. 2014)

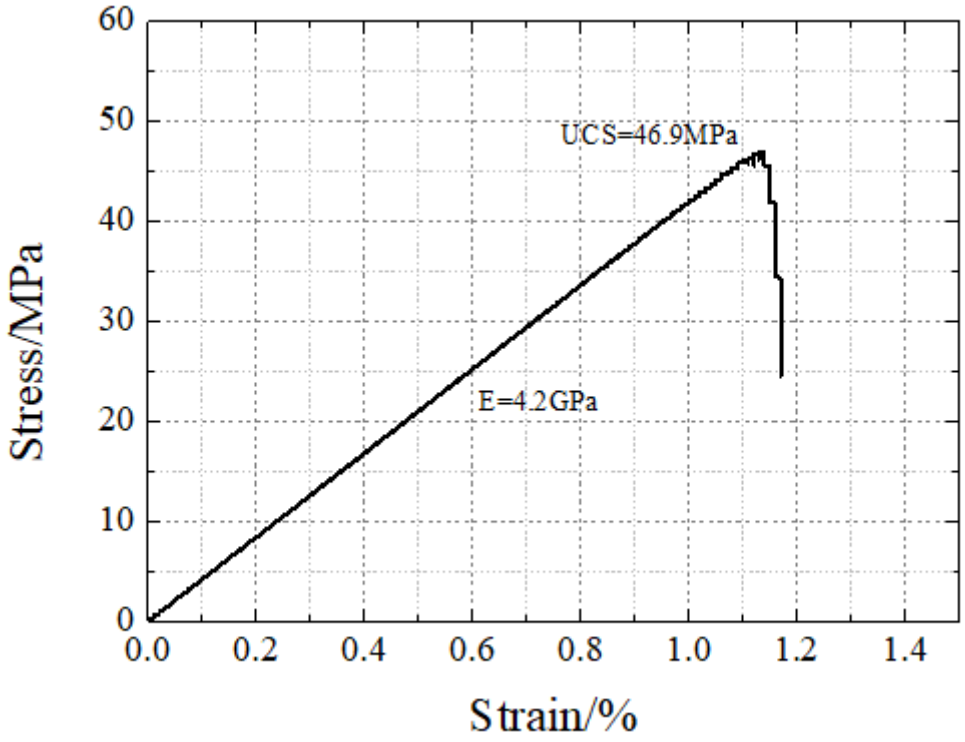

Figure 2

Stress-strain curve of numerical surrounding rock mass

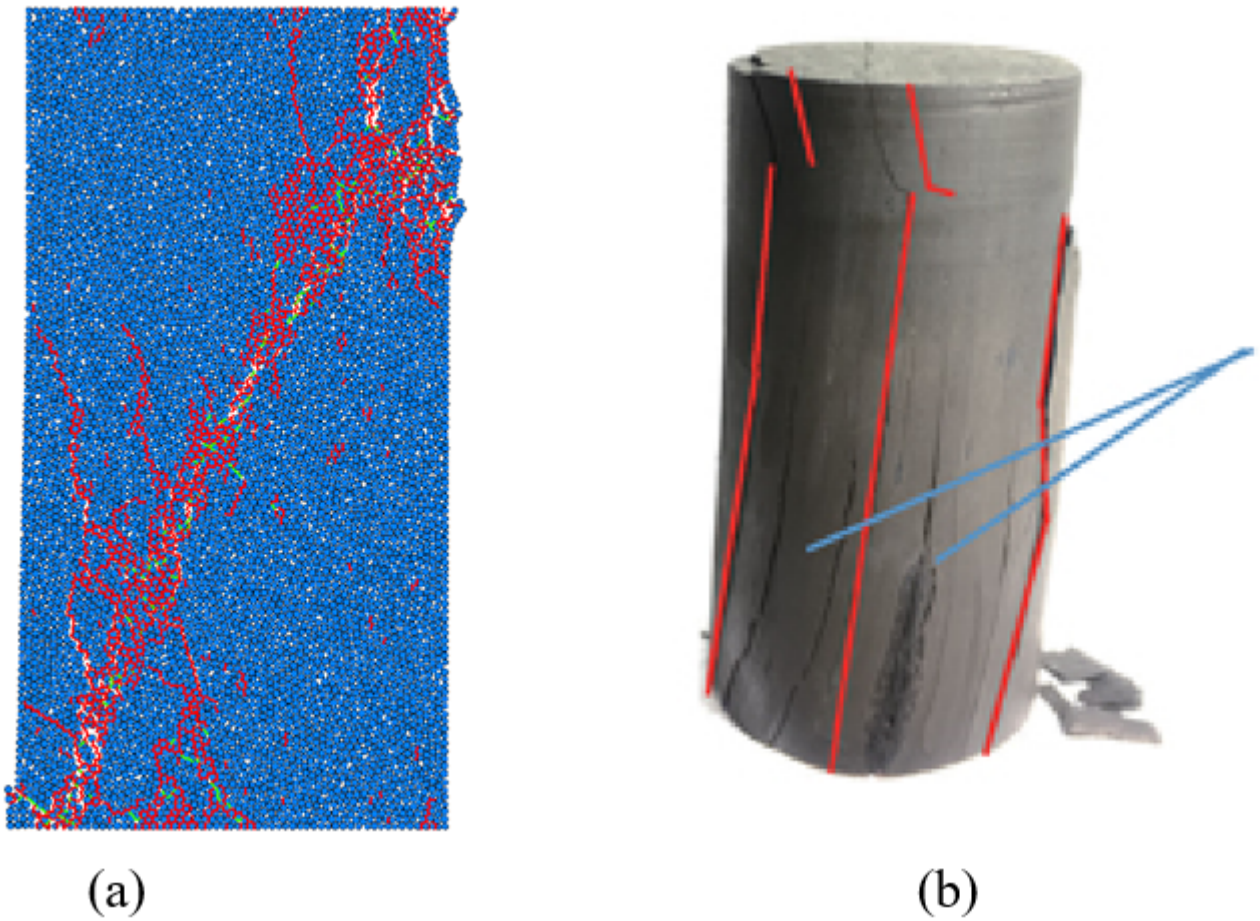

Figure 3

Failure modes of rock samples (a) numerical simulation (b) lab test. Note: red cracks are caused by tensile stress and green cracks are caused by shear stress in numerical model.

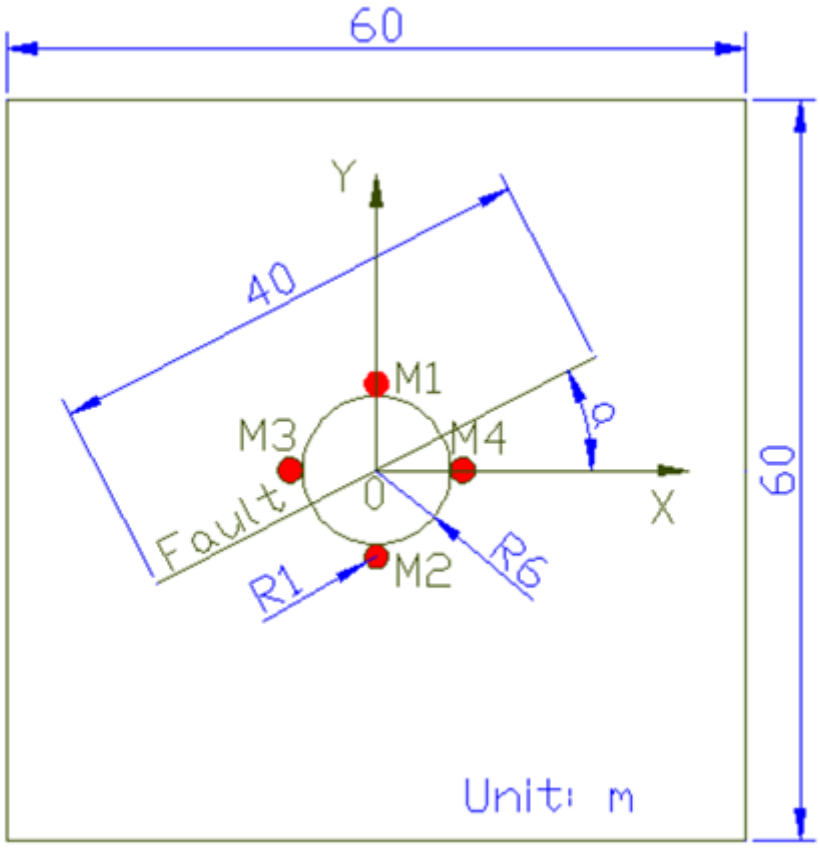

Figure 4

Schematic diagram of cross fault cavern model

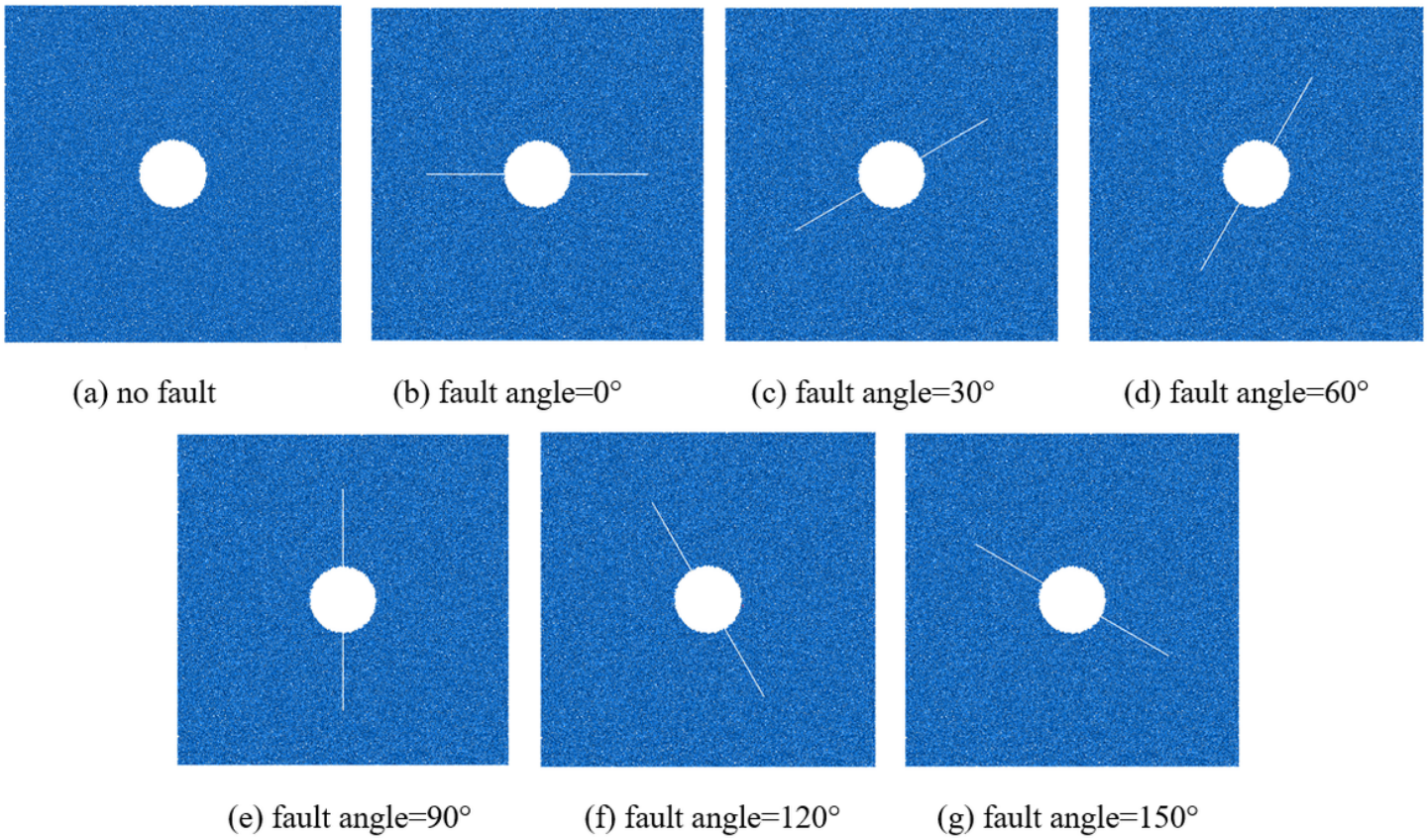

Figure 5

Numerical cross fault cavern models

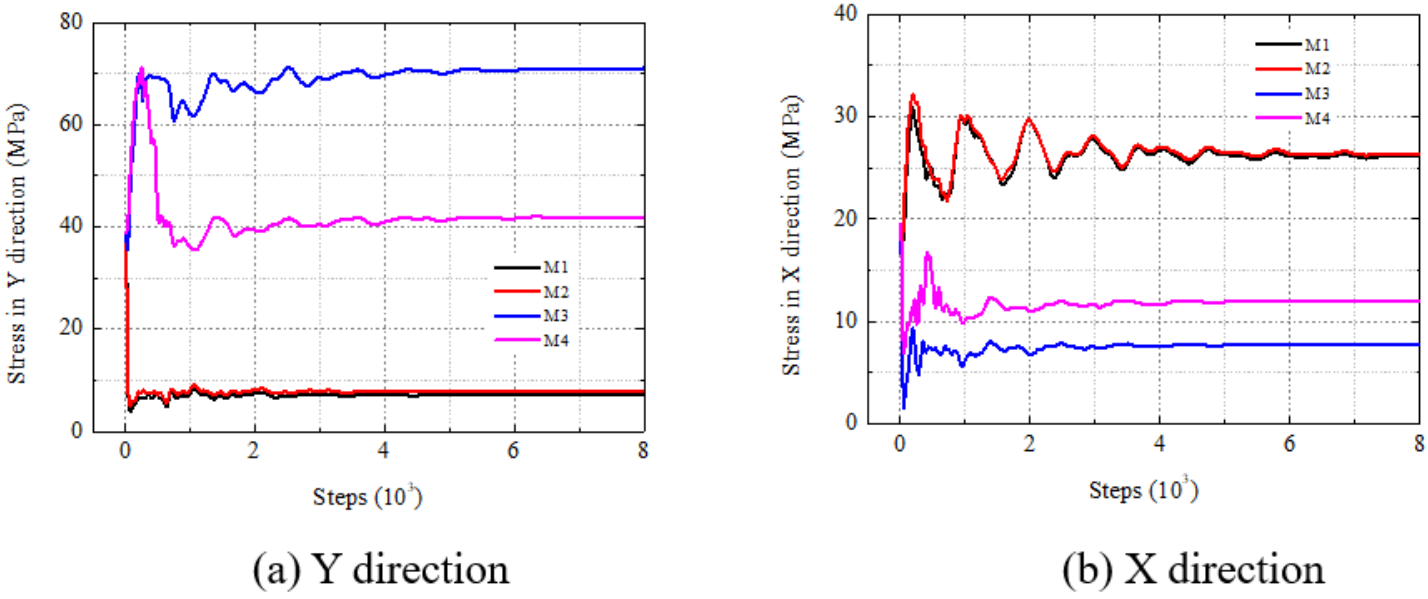

Figure 6

Stress response characteristics of surrounding rock of cavern without fault

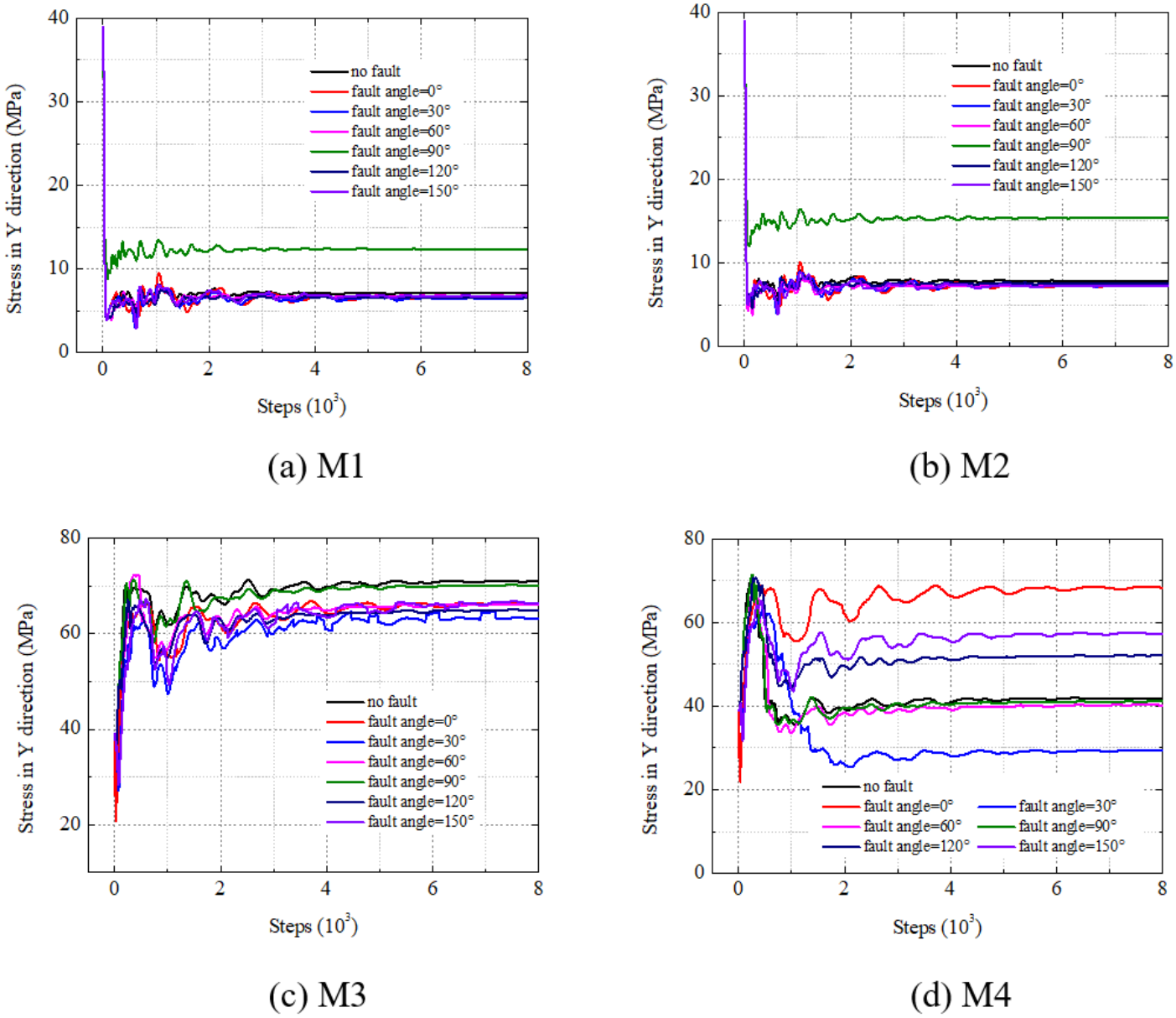

Figure 7

Stress response characteristics of surrounding rock of cavern with fault in Y direction

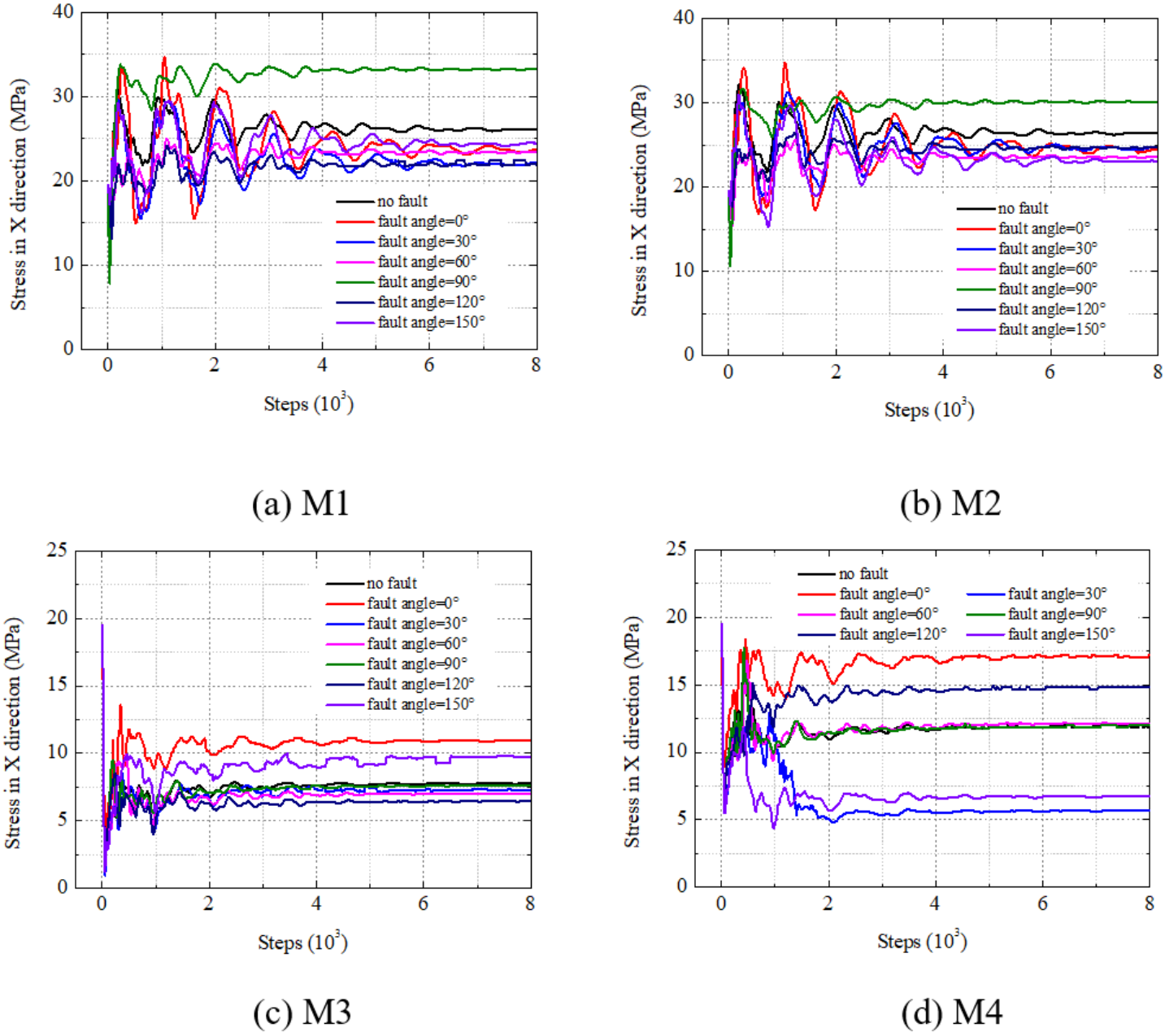

Figure 8

Stress response characteristics of surrounding rock of cavern with fault in X direction

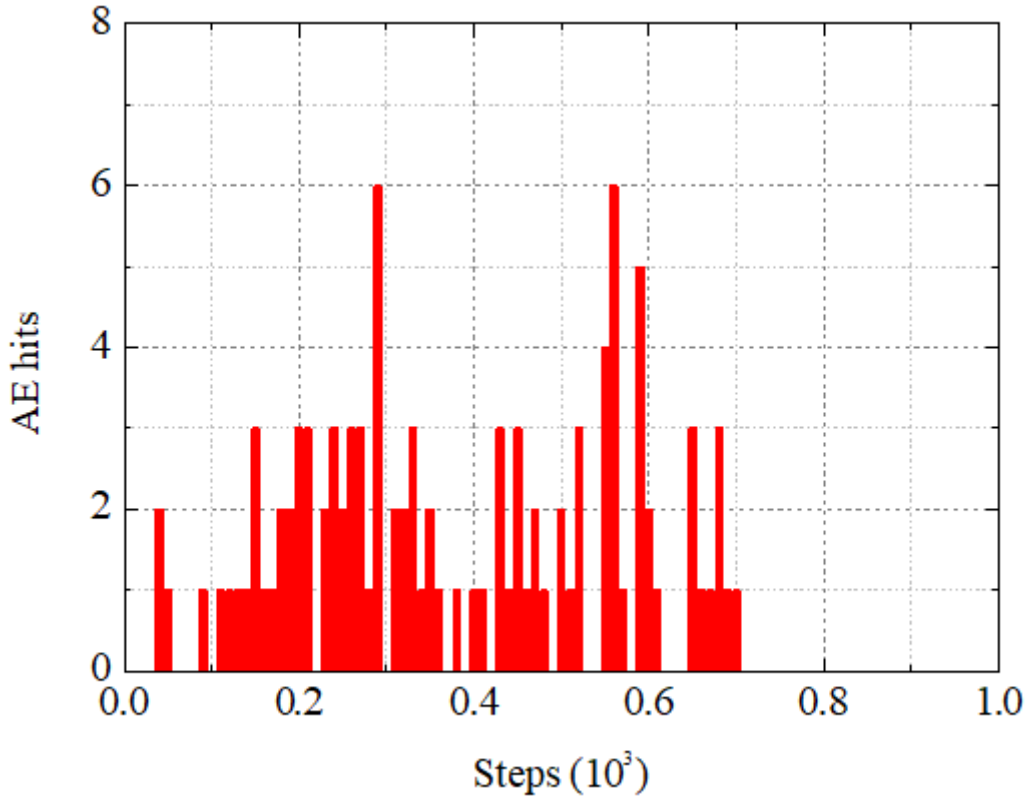

Figure 9

AE characteristics of cavern without fault

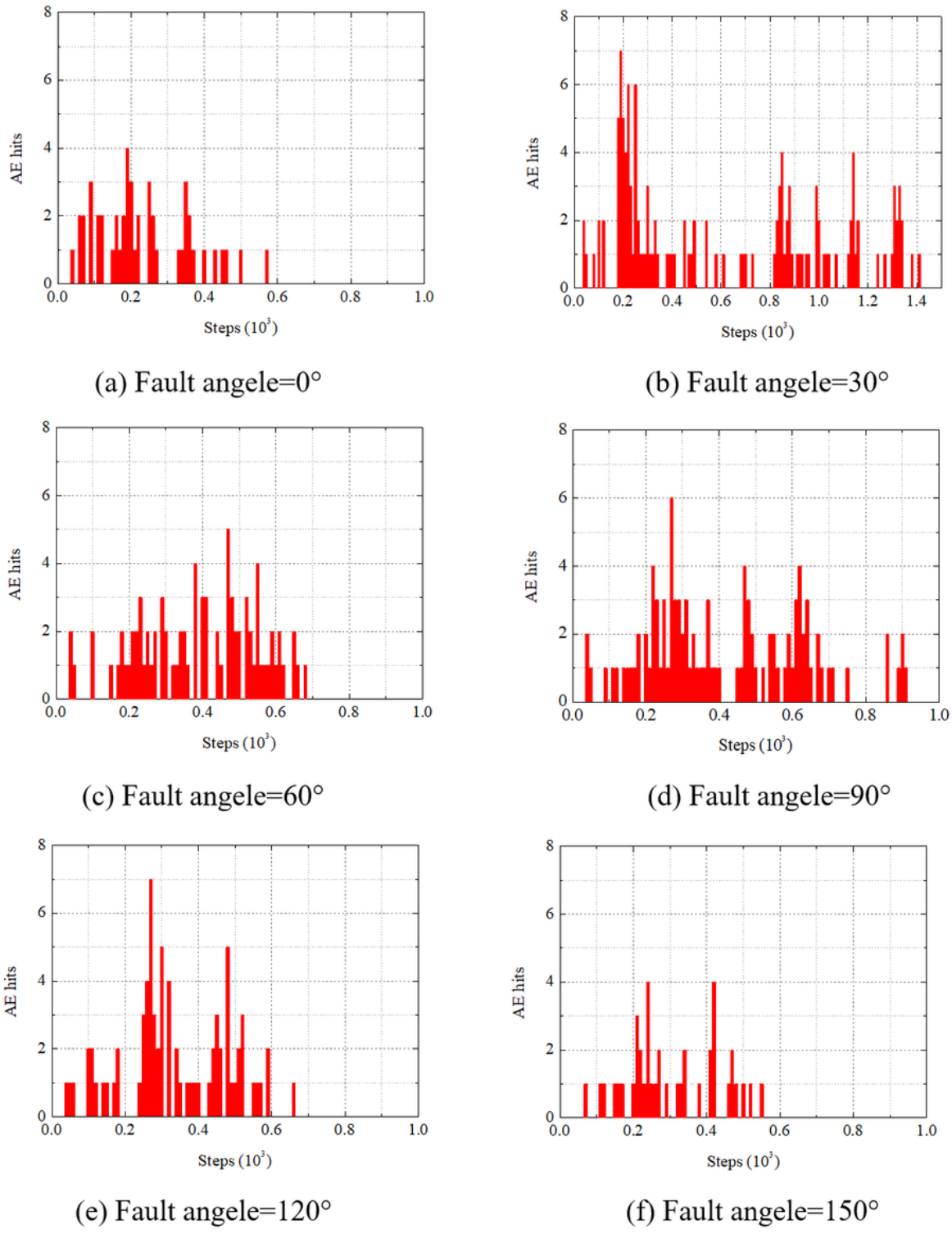

Figure 10

AE characteristics of cavern with different fault angles

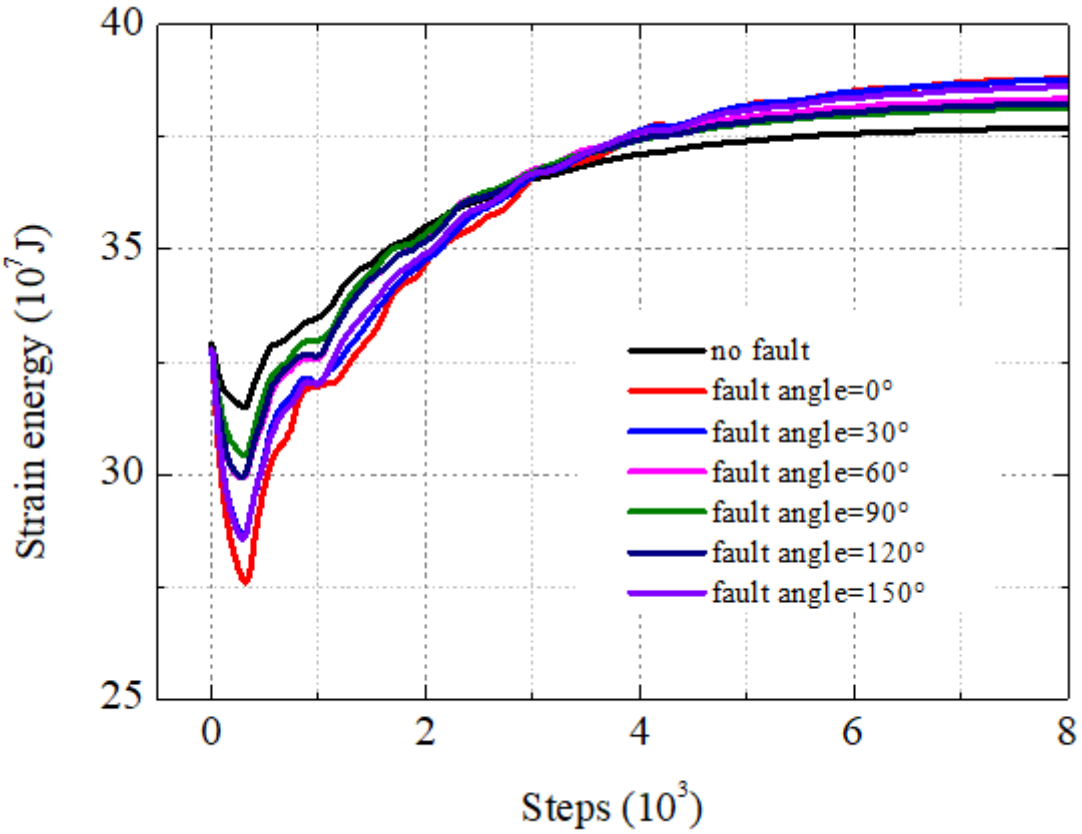

Figure 11

Strain energy characteristics of cavern with different fault angles

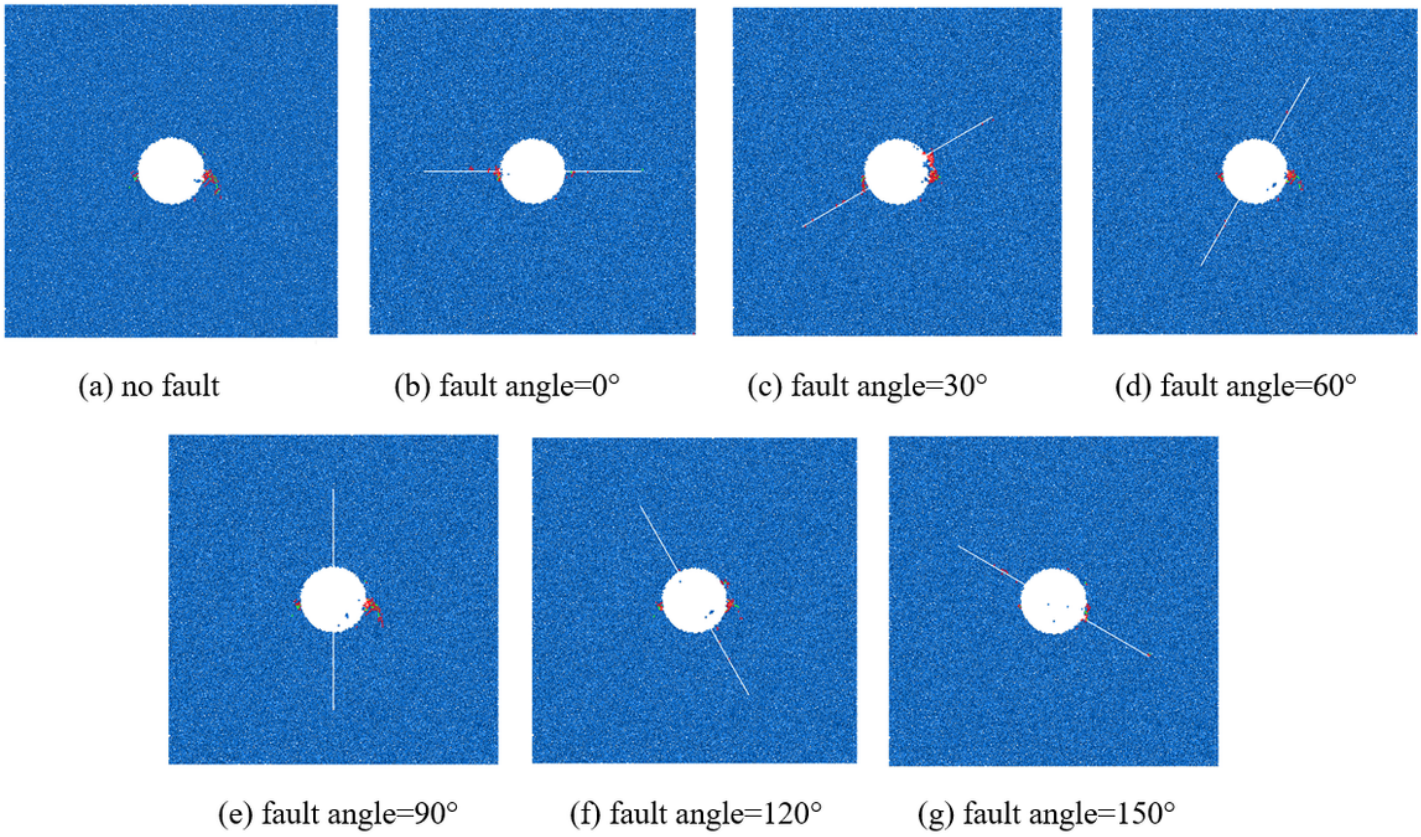

Figure 12

Failure modes of cavern with different fault angles